



## Limits of the quasiharmonic approximation in MgO: Volume dependence of optical modes investigated by infrared reflectivity and *ab initio* calculations

Eugenio Calandrini,<sup>1</sup> Lorenzo Paulatto,<sup>1</sup> Daniele Antonangeli,<sup>1</sup> Fei He,<sup>1</sup> Ricardo P. S. M. Lobo ,<sup>2,3</sup> Francesco Capitani,<sup>4</sup> Jean-Blaise Brubach,<sup>4</sup> Pascale Roy,<sup>4</sup> Laetitia Vincent,<sup>5</sup> and Paola Giura <sup>1,\*</sup>

<sup>1</sup>*Sorbonne Université, Museum National d'Histoire Naturelle, UMR CNRS 7590, Institut de minéralogie, de physique des matériaux et de cosmochimie (IMPMC), 4 place Jussieu, F-75005 Paris, France*

<sup>2</sup>*LPEM, ESPCI Paris, PSL University, CNRS, F-75005 Paris, France*

<sup>3</sup>*Sorbonne Université, CNRS, LPEM, F-75005 Paris, France*

<sup>4</sup>*Synchrotron Soleil, L'Orme des Merisiers Saint Aubin, BP 48 91192 Gif-sur-Yvette, France*

<sup>5</sup>*Université Paris-Saclay, CNRS, Centre de Nanosciences et Nanotechnologie, C2N, Palaiseau 91120, France*



(Received 5 November 2020; revised 18 December 2020; accepted 13 January 2021; published 5 February 2021)

Experimental and numerical investigation of phonon optical modes of MgO as a function of temperature (from 300 to 1400 K) and pressure (from 0 to 21 GPa) are here presented. Infrared reflectivity measurements were performed to probe energies and widths of the optical phonons, as well as of the multiphonon processes affecting the spectral shape, over a variation of the unit-cell volume exceeding 20%. Calculations within quasiharmonic approximation (QHA) account well for the volume dependence of the optical phonon energies observed in high-pressure experiments, while they fail at larger volumes, corresponding to the highest investigated temperatures. Moreover, QHA calculations more closely predict energies of transverse optical (TO) modes than those of longitudinal optical (LO) ones. This can be ascribed to known limitations in the modeling of the effective charges ( $Z^*$ ) and dielectric constant ( $\epsilon_\infty$ ) that lead to an underestimation of the LO-TO splitting. Based on the comparison of our experimental and theoretical results, we propose an empirical analytical expression for  $Z^{*2}/\epsilon_\infty$  as a function of the atomic cell volume. Density-functional perturbation theory including phonon-phonon scattering up to the third order of the lattice potential expansion is used to calculate phonon widths. These calculations reproduce and explain remarkably well the nontrivial volume dependence of both TO and LO phonons linewidths determined by the experiments.

DOI: [10.1103/PhysRevB.103.054302](https://doi.org/10.1103/PhysRevB.103.054302)

### I. INTRODUCTION

Lattice dynamics controls many of the physical quantities responsible for the thermodynamic properties of condensed matter. Among them, we found entropy, thermal capacity, specific heat, thermal expansion, and thermal conductivity [1]. To be able to interpret, predict, and eventually modify these physical quantities in actual materials, is essential to establish an accurate enough model of the force fields, velocities, and scattering rates responsible for atomic movement [2]. This has motivated an advanced treatment of the interatomic potential in which the anharmonic terms are explicitly considered.

Anharmonicity of the interatomic potential leads the interactions between phonons and is therefore responsible for their mutual scattering. Several microscopic descriptions have been developed to explain anharmonic forces and their contribution to intrinsic phonon-phonon scattering processes, either based on experimental data [3], or first-principles approaches [4–10]. However, further refined experiments and advanced calculations are needed to adequately understand multiphonon scattering and its impact on the physical properties of solids [11–16].

To this end, infrared spectroscopy is a first-choice technique to directly address anharmonicity by probing the energy and the lifetime of the infrared active lattice modes. In a purely harmonic picture for diatomic cubic crystals, the infrared absorption spectra should consist of one narrow line. In reality, the measured infrared spectra of cubic crystals show a broad band and at least a secondary band [17]. This discrepancy is qualitatively attributed to anharmonic terms in the potential energy. Thanks to them, the interaction between lattice modes becomes possible, so that a combination of two or more lattice waves can absorb in the infrared region even when the individual waves cannot. Within this context, simple materials, such as the insulating, rocksalt-structured magnesium oxide (MgO) provide an ideal playground, both for experiments (high-quality samples are commercially available) and calculations (with its two atoms per unit cell and six phonon branches it is not computationally demanding, allowing more complex, detailed, and realistic calculations). Furthermore, the stability of MgO, which retains the NaCl (B1) structure over several megabars and thousands of degrees (Ref. [18] and references therein), can be exploited to vary interatomic distances by either pressure or temperature, independently tailoring the phonon-phonon coupling as it will be seen in the following.

An improved understanding of the properties of MgO has also direct implications for Earth and planetary science,

\*Corresponding author: [paola.giura@sorbonne-universite.fr](mailto:paola.giura@sorbonne-universite.fr)

being MgO the compositional end member of ferropericlasite ( $\text{Mg}_{1-x}\text{Fe}_x\text{O}$ ), one of the most abundant constituents of the Earth's lower mantle [19–21] and planetary mantles at megabar pressures [22]. In particular, vibrational properties of MgO and ( $\text{Mg}_{1-x}\text{Fe}_x\text{O}$ ) are directly relevant for the interpretation of lower-mantle seismological observations [23–25] and to model the heat transfer across the planet [4,5,26–28]. In addition, MgO has a technical relevance since it is widely employed as a substrate in chips for THz devices [29].

Despite such a great and diversified interest, MgO vibrational properties as a function of temperature and pressure are relatively poorly known. This paper focuses on the study of the intrinsic phonon-phonon scattering (phonon anharmonicity) and its impact on the normal optical modes in terms of their energies and widths. The evolution with pressure and temperature of these dynamical parameters is here monitored over variations in the unit cell volume of 20% by a combined experimental and theoretical approach. Interestingly, the rearrangement of the phonon density of states at high pressure triggers multiphonon processes that increase the linewidth of the longitudinal modes. Finally, the here-presented methodological approach can be extended to the study of the thermoelastic properties and of the lattice thermal conduction of other insulating crystals of geophysical or technological interest.

## II. METHODS

Infrared reflectivity measurements have been performed on MgO single crystals as a function of temperature and pressures in multiple runs, exploiting different instruments and experimental configurations (see Supplemental Material [30]). High-quality data have been collected between 300 and 1400 K at ambient pressure, and between 0 and 21 GPa at ambient temperature. While measurements covered a larger spectral range, features of current interest locate in the 200 to 1,000- $\text{cm}^{-1}$  range.

Experiments have been complemented by lattice dynamics calculations implemented in the QUANTUM ESPRESSO suite (see Supplemental Material).

## III. EXPERIMENTAL AND COMPUTATIONAL RESULTS

The reflectance spectra of MgO measured as a function of temperature and pressure are shown in Figs. 1(a) and 1(b), respectively. All spectra are characterized by a frequency band of high reflectivity, the so-called reststrahlen band. The transversal and longitudinal optical phonon frequencies at almost zero wave vector,  $\omega_{\text{TO}}$  and  $\omega_{\text{LO}}$ , limit this band. These frequencies relate to the normal modes of lattice vibrations. Outside this spectral region, the reflectivity is constant. The fringes in the high-pressure measurements are due to the multiple internal reflections inside the pressure chamber. The reststrahlen band is perturbed by a shoulder at a frequency slightly lower than  $\omega_{\text{LO}}$ , whose nature goes beyond the quasiharmonic approximation of lattice dynamics, and can be ascribed to anharmonic phonon-phonon interactions as discussed in detail in a recent work [31]. Briefly, this shoulder is the signature of an excess of spectral weight (ESW) due to the decay of a photon with energy  $\hbar\omega_{\text{ESW}}$  and vanishing

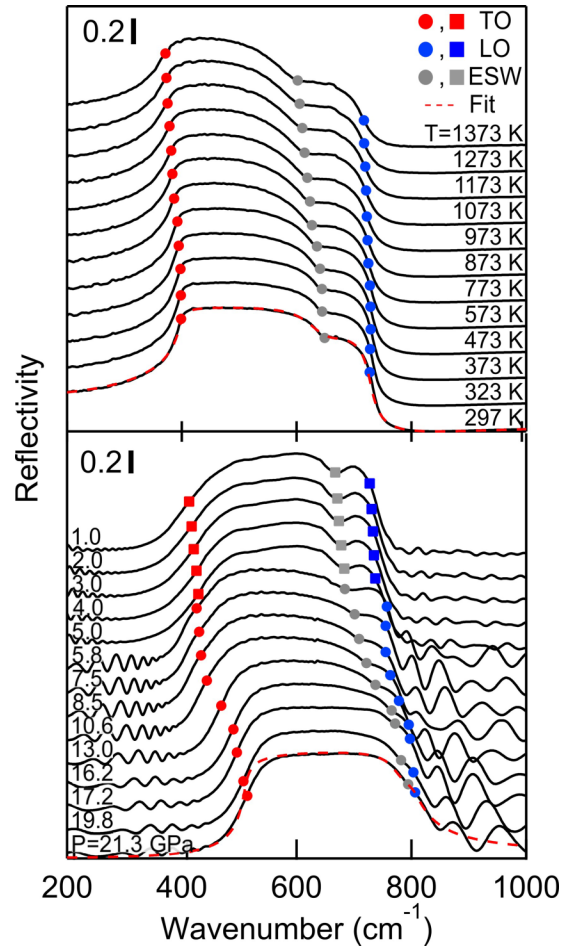


FIG. 1. Reflectivity spectra of MgO single crystal as a function of temperature (top) and pressure (bottom). The curves are all rigidly vertically shifted by the same amount (0.2) for better visibility. The red dashed curves are representative fit results. Red, blue, and gray symbols highlight the position of TO and LO phonons and the ESW feature, respectively. Circles and squares are for different experimental runs.

wave vector ( $q_{\text{in}} \sim 0$ ) in two phonons with opposite wave vector ( $q_{\text{out}}, -q_{\text{out}}$ ), whose energies sum up to  $\hbar\omega_{\text{ESW}}$ . These multiphonon processes are particularly pronounced in ionic compounds, such as MgO, for which the peculiarities of the phononic band structure allow a discretization of the density of state and the onset of pockets, favorable to the phonon-phonon interaction [31].

Overall, spectra undergo a continuous redshift upon increasing temperature and blueshift with increasing pressure. To better highlight this behavior,  $\omega_{\text{TO}}$ ,  $\omega_{\text{LO}}$ , and  $\omega_{\text{ESW}}$  frequencies are marked by colored points in the spectra shown in Fig. 1. A useful way to look at this is by considering, rather than temperature and pressure, the lattice volume, which systematically increases by moving from the bottom to the top of Fig. 1. Qualitatively, phonon softening is commonly expected with increasing interatomic distances. The softening of the ESW energy is a consequence of the general phonon energies shift over the entire reciprocal space, which effectively moves toward lower energies the high phonon density of state pockets responsible for the ESW.

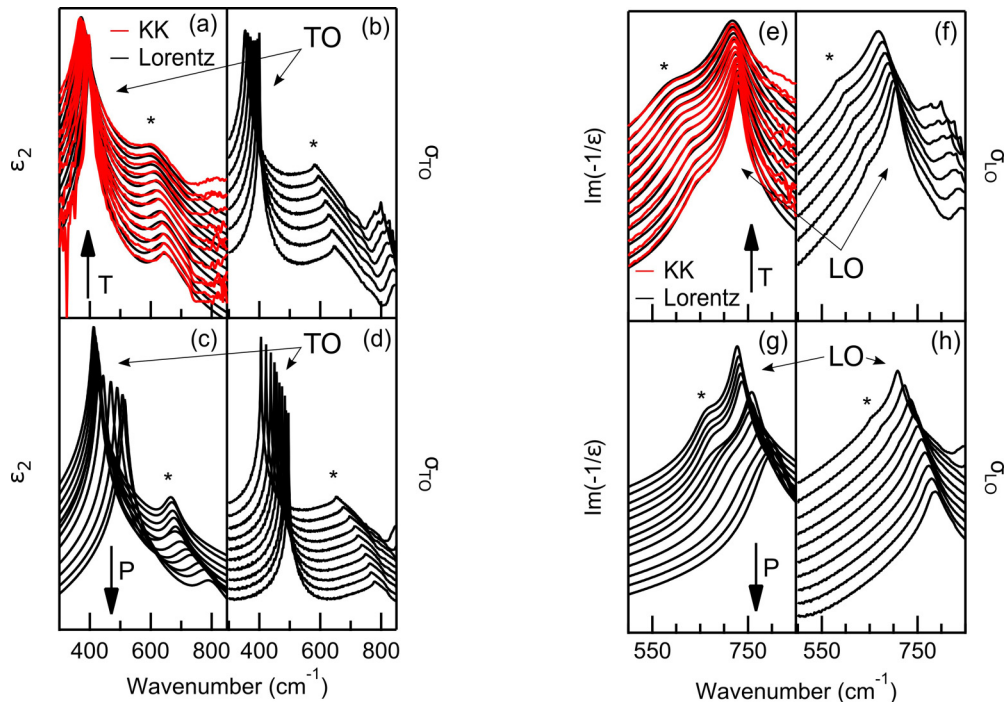


FIG. 2. Experimental and computed optical function of MgO. Panels (a), (c), (e), and (g) show the experimental data analysis results: Lorentz fit (black curves) and Kramers-Kronig analysis (red curves). Panel (a) and panel (c) show the imaginary part of the dielectric function  $\epsilon_2$  at high temperature (a) and high pressure (c). Panel (e) and panel (g) shows the energy loss function at high temperature (e) and high pressure (g). Panels (b), (d), (f), and (h) show the calculated spectral function of TO and LO at high temperature (b), (f) and high pressure (d), (h). N.B. The ordinate axes are in logarithmic scale. Stars (\*) indicate the ESW structure. The main features due to the transverse and to the longitudinal optical phonon are indicated by arrows. Temperature (top panels) increases from the bottom to the top. Pressure (bottom panels) increases from the top to the bottom. Curves are staggered for better visibility.

The thermodynamic behavior of the aforementioned lattice excitations and their lifetimes can be quantitatively described by retrieving the dielectric function of MgO, which directly relates to the refractive index. Results have been analyzed both according to a Lorentz model, and when possible, based on the Kramers-Kronig relation (Supplemental Material [32,33]). As illustrated for the high-temperature measurements [Figs. 2(a)–2(e)], both the Lorentz model (in black) and the Kramers-Kronig relations (in red) capture the relevant features of the dielectric function of the system, and only differ at the edge of the investigated ranges. Concerning the high-pressure measurements, the unavoidable fringes hamper the Kramers-Kronig analysis. As such, in the following, the analysis will be based on the Lorentz model. Representative curves of this fitting procedure are superimposed to the corresponding measured spectra as red dashed lines in Fig. 1. Knowing the dielectric constant, the imaginary part of the energy loss function  $\epsilon_2/(\epsilon_1^2 + \epsilon_2^2)$  provides the frequency and linewidth of LO phonons. The results of this approach are presented in Fig. 2, where  $\epsilon_2$  is shown in panels (a) and (c) and the imaginary part of the energy loss function in panels (e) and (g) for high temperature and high pressure, respectively.

As already mentioned, the peaks' blueshift with decreasing volume (going from top to bottom) is clearly visible. In particular, the ESW peak exhibits a larger shift than the phonons peaks, so that at high pressure it crosses the LO [panel (g)]. The evolution of peak linewidths can also be directly inferred. As expected, a general broadening is observed at high temper-

ature for all the considered excitations. Conversely, TO and ESW linewidths remain constant at high pressure, while the LO linewidths unexpectedly increase.

These experimental results can be directly compared with the density-functional perturbation theory (DFPT) calculations. The resolution of the exact ionic Hamiltonian, using harmonic phonons as the basis, and perturbatively threatening the third order of the total energy approximation, provides corrections to the phonon self-energy, which acquires an imaginary part and confers to the phonons a finite lifetime, i.e., an intrinsic linewidth. The calculated spectral functions of TO and LO phonons take into account these corrections and are displayed in Figs. 2(b)–2(f) and Figs. 2(d)–2(h) for temperatures and pressures between 300 and 1473 K and 0 and 40 GPa, respectively. The agreement with the experiments [in panels (a),(c), (e), and (g) of Fig. 2] is remarkable.

Calculations directly provide the energies and linewidths of normal modes. More interestingly, the analysis of the spectral functions of panels (b), (d), (f), and (h) of Fig. 2 also allows addressing multiphonon processes. Two extra bands, on top of that corresponding to normal models, are well visible. The first (indicated with a star symbol) is the ESW, several orders of magnitude weaker than the normal modes. The second one, further out, is even weaker and highly structured. As the latter lies outside the reststrahlen band, reflectivity measurements are of little use for its investigation, all the more in the case of high-pressure measurements, as the fringes complicate the data interpretation. Thus, while we will discuss

here ESW-related features, we defer the analysis of this second extra band to further dedicated studies. However, it is worth noticing that DFPT calculations can reveal these multiphonon processes, and the discrepancies between the Lorentz model and the Kramers-Kronig analysis at high wave numbers [Figs. 2(a)–2(e)] can be related to the omissions of such processes. The  $\omega_{\text{ESW}}$  frequency is assigned evaluating the local maximum of  $\sigma_{\text{TO}}$  and rapidly crosses the  $\omega_{\text{LO}}$  frequency, as can be seen in panels (f) and (h) of Fig. 2. This complicates the analysis of the imaginary part of the energy loss function because for certain thermodynamic conditions the  $\omega_{\text{LO}}$  and  $\omega_{\text{ESW}}$  modes are closer than the respective linewidths.

Both experimental and numerical results on TO, LO, and ESW are summarized in Fig. 3, where the frequencies and linewidths are displayed as a function of lattice volume (bottom axis) and as a function of temperature and pressure (top axis). The agreement on phonon energies between experiments and calculations, and their smooth, almost-linear dependence on lattice volume, indicate that the quasiharmonic approximation is suitable to describe the lattice dynamics of the system over an extended volume range. Some discrepancies exist concerning LO phonon energy, which result in an underestimation of the theoretically computed LO-TO splitting. This is a known limitation, deriving from the energy functional approximation used to calculate the electronic ground state of the system. However, this problem can be overcome, as discussed later on.

Very differently, the TO and LO phonons linewidths show a nontrivial dependence on the lattice volume [Fig. 3(b)]. Here the anharmonic treatment of the problem is needed to recover the overall behavior of linewidths and its nonmonotonic dependence on lattice volume. Even if the absolute values do not closely match, the increases in the TO and LO phonon linewidths by almost a factor of 3 at large volumes are well reproduced. Noteworthy, since the mismatch is uniform for both the modes, it is conceivable to ascribe this to extrinsic origins. Adding scattering due to isotopic disorder into our calculations does not significantly affect resulting linewidths. Experimentally observed broadening could thus be due to point defects, or other scattering sources.

## IV. DISCUSSION

### A. Modes energies

Figure 3 compares the volume dependence of  $\omega_{\text{TO}}$  and  $\omega_{\text{LO}}$  obtained by experiments and by *ab initio* simulations. Despite the scatter in the experimental data, it is possible to appreciate the good agreement between experiments and QHA simulations up to a critical volume, above which calculations start to deviate from measurements (please refer to Supplemental Material, Fig. S1 for a closer comparison). For the longitudinal phonon, deviation starts at volumes corresponding to room pressure–room temperature measurements, while for the transverse phonon, deviation occurs at higher volumes, indicating a more harmonic behavior with respect to the longitudinal mode. Also, while calculations fit well the experimental transverse energies, longitudinal energies are systematically underestimated. As better addressed in the next section, this is a direct consequence of the difficulties in repro-

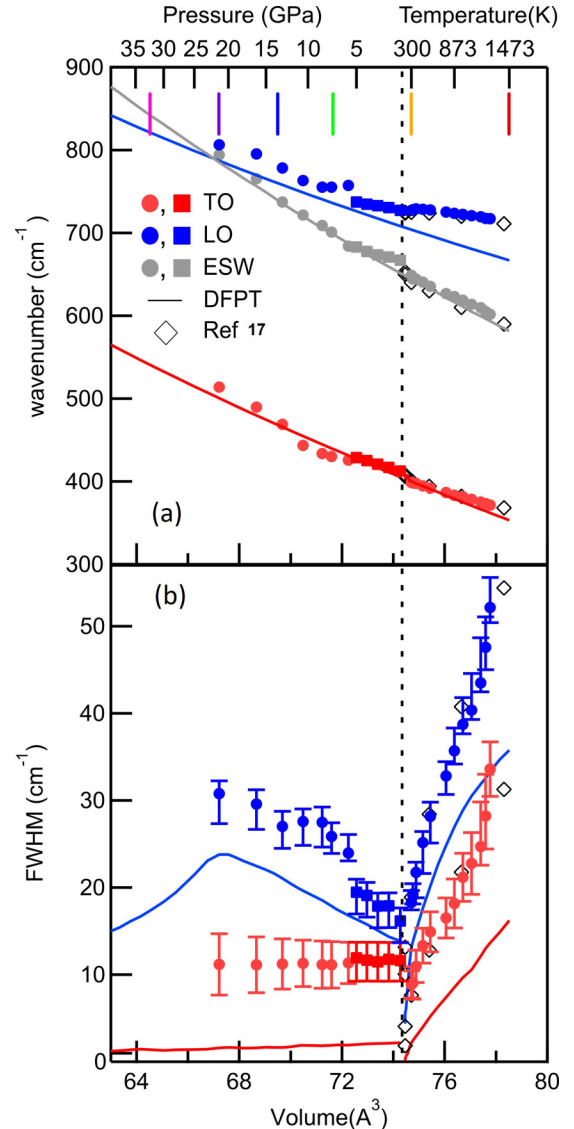


FIG. 3. (a) Phonon energies calculated in the quasiharmonic approximation (lines) and extracted from the Lorentz fit of recorded spectra (circles and squares). (b) Phonon widths calculated including the third order (lines) and extracted from the Lorentz fit of recorded spectra (circles and squares). Literature data from Ref. [17] are reported as open diamonds. Colored markers correspond to  $P$ - $T$  conditions at which we performed phonon DOS and final state calculations reported in Fig. 7. To assign an experimental error, the Lorentz fits were repeated after a rescaling of the measured reflectivity of  $\pm 1\%$ . This procedure reduces any errors caused by the uncertainty on the absolute intensity of the single spectrum and minimizes the effects of misalignment intrinsic to the acquisition of the background. This approach produced the reported error bars for the phonon widths, while no significant effect was produced on the phonon energies.

ducing the effects of the mean local electric field associated with the long-wavelength limit longitudinal phonon.

A first interesting observation that can be made by considering the experimental results at around  $V = 74.1 \text{ \AA}^3$  (gray-shaded area in Fig. S1) is that the energy of the optical modes measured at moderate pressures ( $\sim 1$  GPa) and room

temperature (full circles) is, within uncertainties, the same energy of the optical modes measured for the same volumes, but at ambient pressure and low temperature (<300 K) (open circles from Ref. [33]). As expected within a quasiharmonic approximation, volume seems to be the thermodynamic variable controlling the dynamics, irrespective of actual pressure and temperature conditions leading to this volume. It may therefore be instructive to see over which volume range such observation holds, or in other words, to find the limits above which the quasiharmonic approximation cannot be satisfactorily used anymore.

QHA calculations reproduce well the overall energy-volume relations observed in the high-pressure experiments (but for a rescaling of the absolute values of LO), suggesting that a quasiharmonic approximation holds at ambient temperature at least up to 22 GPa, corresponding to a volume of 67.22 Å<sup>3</sup>. High volumes, obtained for ambient pressure and high temperatures, are more critical, and QHA calculations fail at reproducing the energy-volume relations established by our experiments and available literature data [17]. The difference between experiments and calculations is already sizable at 373 K (74.87 Å<sup>3</sup>) for LO and becomes evident at 773 K (76.05 Å<sup>3</sup>) for TO as well (Fig. 3 and Fig. S1 in Supplemental Material). Thus, the quasiharmonic approximation does not provide an appropriate description of the system at ambient pressure and high temperature.

To further characterize the limits of validity of the quasiharmonic approximation, measurements obtained at constant volume for a different combination of pressure and temperature are necessary (e.g., Ref. [35]). To the same extent, it will be worth to perform perturbative calculations, in particular at high temperature, including both third and fourth orders in the development of the phonon self-energy, which antagonistically contribute to phonon energy determinations, and whose relative weights are expected to depend on actual thermodynamic conditions.

### B. LO-TO splitting

While first-principle calculations well predict the energy of the TO phonons, computed values of the LO energies are systematically below the measured ones (Fig. 3). This problem can be partially solved by empirical corrections based on the analysis of LO-TO splitting.

The LO-TO splitting, i.e., the removal of degeneracy between the LO and TO phonons at the Brillouin-zone center, arises from the breaking of the lattice symmetry by the long-range electric fields associated with long-wave longitudinal phonons. This effect can be accounted for in the dynamical matrix as  $q \rightarrow 0$ , introducing a nonanalytic contribution given by

$$\frac{4\pi}{V} e^2 \frac{(qZ_i^*)_\alpha (qZ_j^*)_\beta}{q\epsilon_\infty q}, \quad (3)$$

where  $V$  is the volume of the primitive cell,  $Z_{i(j)}^*$  is the Born effective charge tensor for the  $i(j)$ th atom,  $\epsilon_\infty$  is the high-frequency static dielectric tensor, and  $e$  is the electronic charge. Thus, the knowledge of the tensor  $z^*$  of the Born effective charges and the tensor  $\epsilon_\infty$  of the macroscopic high-frequency dielectric constant is needed to correctly describe

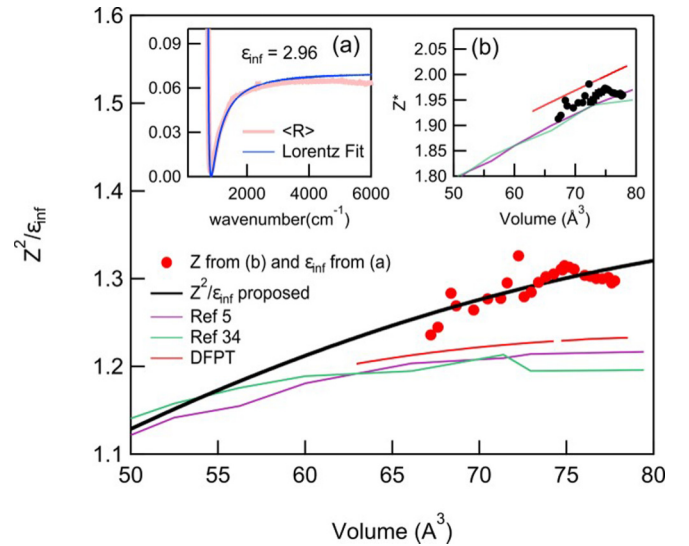


FIG. 4. Ratio  $Z^{*2}/\epsilon_\infty$  as a function of volume. The estimation from experimental results (dots) is compared to estimations from the *ab initio* simulations (thin lines) performed in this study (DFPT) and available in the literature [5,34]. Inset (a): Lorentzian fit (blue line) of the high-energy trend of the mean reflectivity curve  $\langle R \rangle$  (red line). Inset (b): effective charge number  $Z^*$ .

the dynamical matrix at the Brillouin-zone center. Actually, the ratio  $Z^{*2}/\epsilon_\infty$  controls the magnitude of the LO-TO through the relation

$$\frac{Z^{*2}}{\epsilon_\infty} = \frac{\mu V}{4\pi e^2} (\omega_{LO}^2 - \omega_{TO}^2), \quad (4)$$

where  $\mu$  is the reduced atomic mass and  $V$  the volume of the unit cell. The values for  $Z^*$  and  $\epsilon_\infty$  can be self-consistently calculated in the framework of DFPT, but also derived from the experiments. In the latter case, the high-frequency dielectric constant is a fit parameter, while the Born effective charges can be determined by the following relation:

$$Z^{*2} = \frac{\mu V S \omega_{TO}^2}{4\pi e^2}, \quad (5)$$

where  $\mu$  is the reduced mass of MgO,  $V$  is the volume of the unit cell,  $S$  and  $\omega_{TO}^2$  are, respectively, the oscillator strength and frequency of the transverse phonon, and  $e$  is the electronic charge.

Figure 4 compares the measured and calculated values for  $Z^*$ , the tensor  $\epsilon_\infty$ , and the ratio  $Z^{*2}/\epsilon_\infty$ . In particular, the  $Z^{*2}/\epsilon_\infty$  experimental values shown in Fig. 4 are obtained by the Lorentz model analysis used to estimate:

(i) the mean value of the high-frequency dielectric constant,  $\epsilon_\infty$  [Fig. 4, inset (a)] from the high-energy trend of the mean reflectivity curve obtained by averaging the experimental data at the different volumes.

(ii) the effective charge number  $Z^*$  [Fig. 4, inset (b)] from the transverse optic phonon oscillator strength.

Despite that the present *ab initio* calculations plot closer to the experimental determination than previous work [5,34], computed  $Z^{*2}/\epsilon_\infty$  are systematically below the experimental values. This discrepancy mostly comes from the overestimation of the high-frequency dielectric constant and not from the

Born effective charge [inset (b) of Fig. 4], as also evidenced by the systematic underestimation of the longitudinal optical mode energy shown in Fig. 3. In particular, all theoretical models underestimate the increasing LO-TO splitting with increasing volume.

To improve the accuracy of the theoretical modeling and to minimize the difference with respect to measurements, a  $Z^{*2}/\epsilon_\infty$  ratio scaled on the experimental data can be treated as an external input parameter for the calculations. Starting from a polynomial fit to the experimental values (bold thick black line in Fig. 4), we can define an empirical analytical expression for  $(Z^{*2}/\epsilon_\infty)_{\text{exp}}$  as a function of the atomic unit-cell volume  $V$ :

$$(Z^{*2}/\epsilon_\infty)_{\text{exp}}(V) = 0.4(2) + 1.9(1) \times 10^{-2} V - 9.7(4) \times 10^{-5} V^2. \quad (6)$$

Such empirical scaling is neither meant to replace more advanced treatments of the dynamical matrix in the limit of  $q \rightarrow 0$ , nor of the Born effective charge tensor over an extended pressure or temperature range. Here we simply aim at providing an analytical correction to be applied to estimation of the LO-TO splitting by quasiharmonic calculations over the here-considered volume range, and within the limit of a quasiharmonic approach.

### C. Grüneisen parameters

A classic, but still largely used way to describe and to quantify anharmonicity is through the Grüneisen parameter ( $\gamma$ ) [36]. In this microscopic picture of the lattice dynamics, atomic oscillations are controlled by a pair potential energy containing an attractive and a repulsive term, which depend on the relative mean distance between the atoms. At finite, but relatively low temperature, the atomic displacement is sufficiently small with respect to the interparticle distances, so that the potential energy around the equilibrium position could be satisfactorily approximated by a parabola giving rise to an elastic recovering force (pure harmonic model). In the Grüneisen description, the equilibrium position is a function of temperature and pressure to account for the volume variation caused by thermal expansion or by compression (*quasi*-harmonic approximation). Noteworthy, in this model the only influence of pressure and temperature on the vibrational frequency comes from the effect that these have on the interatomic equilibrium position, or in other terms, on the volume  $V$ . These arguments and approximations lead to the classically used equations:

$$\frac{1}{v} \frac{\partial v}{\partial T} = -\gamma \frac{1}{V} \frac{\partial V}{\partial T}, \quad (7)$$

$$\frac{1}{v} \frac{\partial v}{\partial P} = -\gamma \frac{1}{V} \frac{\partial V}{\partial P}, \quad (8)$$

$$-\frac{\partial \ln(v)}{\partial \ln(V)} = \gamma, \quad (9)$$

where  $\gamma$  is the Grüneisen parameter that can be written for every phonon mode as follows:

$$\gamma_i = -\frac{\partial \ln(v_i)}{\partial \ln(V)}, \quad (10)$$

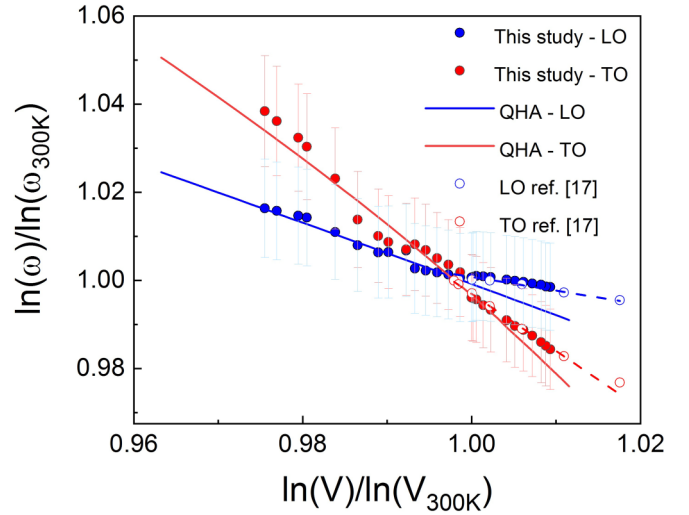


FIG. 5. Natural logarithm of the phonon energy  $\omega_{\text{LO}}$  (red) and  $\omega_{\text{TO}}$  (blue) as a function of  $\ln(V)$  for high-pressure and high-temperature measurements (dots) and QHA calculations (solid lines). Linear fits for the high-volume (HV) experimental data, there where the QHA calculations do not account for the experimental observations anymore, are displayed as dashed lines with consistent color coding.

where  $v_i$  refers to the frequency of the  $i$ th phonon mode.

From a macroscopic standpoint, the Grüneisen parameter is defined as [37]

$$\gamma = \frac{\alpha K_T V}{C_V} = \frac{\alpha K_S V}{C_p}, \quad (11)$$

where  $K_T$  ( $K_S$ ) is the isothermal (adiabatic) bulk modulus,  $\alpha$  is the thermal expansion coefficient, and  $C_V$  ( $C_p$ ) is the specific heat at constant volume (pressure). From Eq. (11), one can see that the Grüneisen parameter sets a link between the thermal and the elastic properties of a solid.

Figure 5 shows the natural logarithm of the phonon energy of the optical modes probed in this study,  $\ln(\omega_{\text{LO}})$  (red) and  $\ln(\omega_{\text{TO}})$  (blue), as a function of  $\ln(V)$  for both high-pressure and high-temperature ranges. To facilitate comparison, quantities are rescaled to their respective values at ambient conditions, i.e.,  $T = 300$  K and  $P = 1$  atm ( $V = 74.704 \text{ \AA}^3$ ,  $\omega_{\text{LO}} = 727 \text{ cm}^{-1}$ , and  $\omega_{\text{TO}} = 400 \text{ cm}^{-1}$ ). At high pressures (low volumes) QHA calculations well account for the observations, within the scatter of the data. Conversely, a departure from the quasiharmonic model can be noticed at high temperature, with increasing volumes, at first for LO, then for TO. Over this volume range, both LO and TO data can be well described by a linear fit (dashed lines in Fig. 5), whose slope is less steep than what is expected according to QHA calculations.

It can also be readily observed that the energy of the transverse mode has a more pronounced dependence on the volume than the energy of the longitudinal one. This can be rationalized by considering the effect of atomic distances on the Coulomb force associated with the long-range electric fields at the origin of the LO-TO splitting: with increasing/decreasing interatomic distances (increasing/decreasing volume) the Coulomb force decreases/increases.

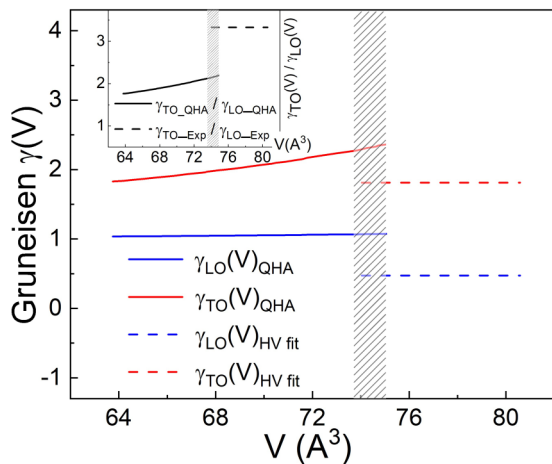


FIG. 6. Grüneisen parameters for LO (blue) and TO (red) phonons as a function of volume. Continuous lines are QHA results; dashed lines are obtained by the derivative of the fits to the experimental data at the high volumes (dashed lines in Fig. 5). The shaded region highlights the HV range over which QHA calculations progressively deviate from experimental observations. Inset: TO/LO Grüneisen parameters ratio.

The greater hardening of the TO mode with decreasing volume is also clearly described by the Grüneisen parameter, calculated according to Eq. (10), and whose trend with volume is reported in Fig. 6. In the volume range where QHA calculations well describe the measurements,  $\gamma(V)_{\text{QHA}}$  follows a quadratic law much more pronounced for the transverse optical phonon than for the longitudinal one. At higher volumes, we estimated the mode Grüneisen parameters starting from the linear fit to the experimental data (dashed lines in Fig. 5). In this volume range,  $\gamma_{\text{TO}}$  is more than three times  $\gamma_{\text{LO}}$ .

By looking at Fig. 6, it is possible to remark that within the quasiharmonic approach, Grüneisen parameters decrease with reducing volume. Such behavior is consistent with high-pressure measurements, but it becomes soon inadequate for the high-temperature measurements. At the high volumes, corresponding to the highest-temperature conditions,  $\gamma(V)$  strongly decreases for both modes while the relative ratio between  $\gamma(V)_{\text{TO}}/\gamma(V)_{\text{LO}}$  increases (see inset in Fig. 6).

Quantitatively, although with a discontinuity likely less sharp than that schematically illustrated in Fig. 6, the Grüneisen parameter for the longitudinal phonon goes from  $\sim 1$  to  $\sim 0.3$ , a value three times smaller, while that of the transverse phonon changes by less than half passing from  $\sim 2.2$  to  $\sim 1.3$ .

This drastic reduction of the Grüneisen parameter relates to the increased anharmonic contributions. Interestingly, as shown in Fig. 3, the measured phonon's energies, and in particular those of the LO mode, are higher than what is expected according to the QHA predictions. Both the third and fourth terms of the interatomic potential contribute to the real part of the phonon self-energy, respectively, decreasing and increasing the phonon energies. There where QHA calculations well predict phonon energies, the two terms of higher order compensate each other. Our results suggest that for increasing temperature, cubic and quartic terms of the

crystal Hamiltonian do not compensate anymore, with the progressive prevalence of the latter one. Further, more extensive perturbative calculations over an extended temperature range will be necessary to quantitatively confirm this hypothesis.

#### D. Mode linewidths

The evolution of phonon widths with volume [Fig. 3(b)] shows two different trends for high-pressure and high-temperature data. The discontinuity observed for both the optical modes' widths seems located near ambient conditions.

In the high-temperature regime, the widths of the phonons increase monotonically because thermal energy allows atoms to move away from their equilibrium positions, exploring the actual shape of the lattice potential beyond the quadratic well. In other words, by increasing temperature, it is possible to check the degree of anharmonicity of the system and the weight of higher-order energy terms. In general, it has been observed that the temperature dependence of the phonons' widths on the third and fourth order of the potential expansion has different trends. For the former the trend becomes linear over a few tens of Kelvin, while no linearity is observed for the latter as accurately shown in a recent work where calculations are done up to temperatures around 1000 K at room pressure [38]. In our case, the high-volume experimental data, i.e., high-temperature and room-pressure phonon widths, reported in Fig. 3(b), exhibit a linear behavior on temperature that is maintained up to 2000 K when adding literature data [17] (please see Supplemental Material, Fig. S2 for an extended view). This would suggest that four-phonon scattering has not a strong effect. However, the discrepancy between measured and computed data is not constant on temperature, differently from that observed on pressure. Moreover, the computed linewidths for the LO phonon show a clear deviation from linearity for temperatures higher than 1000 K. These findings support the hypothesis that the four-phonon scattering becomes non-negligible with increasing temperature at room pressure not only for phonon energies, as discussed in the previous section, but also for phonon widths with a particular weight for the highest-energy modes.

Compared with temperature, high pressure could be speculated to have an opposite effect, reducing interatomic distances, and enhancing the repulsive component in the interatomic potential, and hence, in some way, increasing the harmonic character of the collective vibrations. This is qualitatively compatible with the almost constant or slight decrease of the width of the TO mode with decreasing volume caused by the increasing pressure. However, this is not the case for the LO mode, which shows an evident nonmonotonic increase with decreasing volume, with a maximum width when LO energy matches that of ESW. This picture becomes clear once combining the theoretical and experimental results. The calculated MgO phonon density of states (DOS) reported in Fig. 7 features two main energy pockets, one highly populated by phonon states belonging to TO and LA branches, the other by phonons belonging to TA branches, which all display a nearly flat dispersion (please refer to Ref. [31] for phonon dispersions and a more detailed description).

These two energy pockets, which evolve following the phonon band structure, i.e., blueshift decreasing the cell

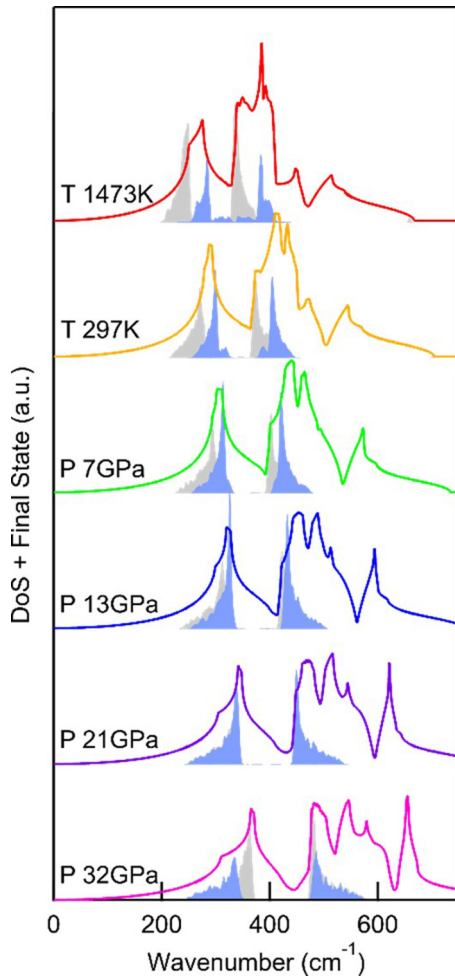


FIG. 7. Evolution of the phonon DOS with the thermodynamic conditions. The color coding is consistent with marks in Fig. 3. The blue- (gray)-shaded zone represents the final states of the LO (ESW) decay process.

volume, host the final states of multiphonon decay processes (almost irrespective of the actual exchange momentum).

If a particle, be this a photon or a phonon, possesses an energy equal to the sum of these two energies it can decay, generating two phonons: this is what happens to the LO phonon or to photons having the ESW energy. At ambient conditions, the energies of the two pockets sum up to  $650\text{ cm}^{-1}$ , and only photons satisfy the energy (and momentum) conservation. As the pressure increases, the band structure rearranges; the ESW approaches the LO energy that eventually matches the sum of the DOS energy pockets, thus providing an effective channel for the LO phonon to decay. The direct consequence is a progressive decrease in the LO lifetime that manifests with the observed increase in the linewidth. At the best energy matching, final states of ESW and LO decay processes superimpose ( $21\text{ GPa}$ ,  $790\text{ cm}^{-1}$ ) and the LO width goes through a maximum. As the pressure further increases, the LO energy detunes, and its width reduces. In conclusion, the presence of these pockets in the DOS, whose energy combination is tuned with one of the normal lattice modes, triggers multiphoton decay processes. The presence of such multiphoton processes increases the

linewidth of normal modes and hence the anharmonicity of the lattice dynamics even at high pressure, where the stiffer and more packed environment should result in more harmonic lattice dynamics (e.g., Ref. [35]).

## V. CONCLUSIONS

In this paper, we present a thorough experimental and numerical investigation of phonon optical modes of MgO as a function of temperature (from 300 to 1400 K) and pressure (from 0 to 21 GPa). The infrared reflectivity measurements complement previous datasets [17,39], allowing for a more detailed analysis, in particular at high pressure. Both phonon energies and phonon widths of three active phonon processes (LO, TO, and ESW, an excess of spectral weight caused by multiphonon processes) are probed over a variation of the unit-cell volume exceeding 20%. The experimental results provide a critical testbench for the *ab initio* simulations.

While the theoretical approach is overall validated in terms of optical phonon energy positions, calculations work better for TO than for LO. This can be ascribed to known limitations in the modeling of the effective charges and dielectric constant that lead to underestimation of the LO-TO splitting in MgO. Based on the comparison of our experimental and theoretical results we propose an empirical analytical expression for  $Z^{*2}/\epsilon_\infty$  as a function of the atomic unit-cell volume  $V$  to rescale results from quasiharmonic calculations.

Calculations within QHA account well for the volume dependence of the optical phonon energies observed in high-pressure experiments but fail both for TO and LO at larger volumes, corresponding to the highest investigated temperature. Higher-order, nonharmonic terms in the crystal Hamiltonian become necessary, with the quartic term expected to dominate over the cubic one.

Phonon widths were calculated beyond a quasiharmonic approximation, including phonon-phonon scattering up to the third order of the lattice potential expansion. The results of these calculations reproduce remarkably well the nontrivial dependence on the lattice volume of both TO and LO phonons' linewidths highlighted by the experiments. Even if the absolute values do not closely match, the increase in the linewidths by almost a factor of 3 at large volumes is well captured. Furthermore, the almost constant mismatch suggests it might have an extrinsic origin. Interestingly, the calculations allow explaining the maximum in LO phonon widths versus pressure at around 21 GPa as the consequence of the progressive opening and closing of phonon decay channels, triggered by the energy of the ESW approaching and moving out that of LO phonon.

The highly nonlinear evolution of phonon linewidth with volume could have important consequences for the lattice thermal conduction of MgO. More generally, predictions of lattice conduction of insulating crystals of geophysical interest based on a quasiharmonic approach might fail at providing reliable estimates, as more complex models are required to properly describe lattice dynamics.

Looking further in perspective, peculiar band structures such as those of MgO can be reverse engineered to tailor the desired set of final states and hence trigger decay processes of a given phonon branch, eventually at a given  $k$



point of the reciprocal space. These customized materials will find applications based on fine control of the lattice transport properties in a given energy (temperature) range or along a given direction. Additionally, the temperature evolution of the band structure could be further exploited to set a temperature threshold for the activation/deactivation of the aforementioned decay processes.

All these fascinating applications call for an improved understanding of the anharmonic mechanisms controlling lattice vibrations.

### ACKNOWLEDGMENTS

The authors wish to thank Benoit Baptiste for single-crystal alignment. This work was supported by the Investisse-

ments d’Avenir programme (Reference No. ANR-11-IDEX-0004-02) and more specifically within the framework of the Cluster of Excellence MATeriaux Interfaces Surfaces Environnement (MATISSE) led by Sorbonne Université, by the China Scholarship Council–Sorbonne Université program for doctoral scholarships, and by the Conseil Régional d’Île-de-France through the DIM OxyMORE. HPC resources are granted under the GENCI Allocation No. A0030907320. Femtosecond laser micromachining at the Institut de Minéralogie de Physique des Matériaux et de Cosmochimie (IMPMC), Paris has been developed and realized by the “Cellule Project” with the financial support of Grant No. ANR 2010-JCJC-604-01. Infrared measurements were recorded during the accepted Proposals No. 20151247 and No. 20191644 on the Ailes beamline of synchrotron SOLEIL.

- 
- [1] T. M. Tritt, *Thermal Conductivity* (Springer, Boston, 2004).
- [2] R. A. Cowley, *Adv. Phys.* **12**, 421 (1963).
- [3] A. M. Hofmeister, *Science* **283**, 1699 (1999).
- [4] N. De Koker, *Phys. Rev. Lett.* **103**, 125902 (2009).
- [5] N. de Koker, *Earth Planet. Sci. Lett.* **292**, 392 (2010).
- [6] X. Tang and J. Dong, *Proc. Natl. Acad. Sci. USA* **107**, 4539 (2010).
- [7] Y. Shen, C. N. Saunders, C. M. Bernal, D. L. Abernathy, M. E. Manley, and B. Fultz, *Phys. Rev. Lett.* **125**, 085504 (2020).
- [8] L. Lindsay, C. Hua, X. L. Ruan, and S. Lee, *Mater. Today Phys.* **7**, 106 (2018).
- [9] F. Soubiran and B. Militzer, *Phys. Rev. Lett.* **125**, 175701 (2020).
- [10] T. Feng, L. Lindsay, and X. Ruan, *Phys. Rev. B* **96**, 161201 (2017).
- [11] W. Wan, Y. Ge, and Y. Liu, *Appl. Phys. Lett.* **114**, 031901 (2019).
- [12] Y. Oba, T. Tadano, R. Akashi, and S. Tsuneyuki, *Phys. Rev. Mater.* **3**, 033601 (2019).
- [13] D. Tristant, A. Cupo, X. Ling, and V. Meunier, *ACS Nano* **13**, 10456 (2019).
- [14] F. Liu, P. Parajuli, R. Rao, P. C. Wei, A. Karunaratne, S. Bhattacharya, R. Podila, J. He, B. Maruyama, G. Priyadarshan, J. R. Gladden, Y. Y. Chen, and A. M. Rao, *Phys. Rev. B* **98**, 224309 (2018).
- [15] Y. K. Peng, Z. Y. Cao, L. C. Chen, N. Dai, Y. Sun, and X. J. Chen, *J. Phys. Chem. C* **123**, 25509 (2019).
- [16] R. Peierls, *Ann. Phys.* **395**, 1055 (1929).
- [17] J. R. Jasperse, A. Kahan, J. N. Plendl, and S. S. Mitra, *Phys. Rev.* **146**, 526 (1966).
- [18] J. Bouchet, F. Bottin, V. Recoules, F. Remus, G. Morard, R. M. Bolis, and A. Benuzzi-Mounaix, *Phys. Rev. B* **99**, 094113 (2019).
- [19] Y. Zhao and D. L. Anderson, *Phys. Earth Planet. Inter.* **85**, 273 (1994).
- [20] E. Mattern, J. Matas, Y. Ricard, and J. Bass, *Geophys. J. Int.* **160**, 973 (2005).
- [21] B. Li and J. Zhang, *Phys. Earth Planet. Inter.* **151**, 143 (2005).
- [22] D. Valencia, R. J. O’Connell, and D. Sasselov, *Icarus* **181**, 545 (2006).
- [23] H. Marquardt, S. Speziale, H. J. Reichmann, D. J. Frost, F. R. Schilling, and E. J. Garnero, *Science* **324**, 224 (2009).
- [24] F. Cammarano, H. Marquardt, S. Speziale, and P. J. Tackley, *Geophys. Res. Lett.* **37**, 03308 (2010).
- [25] D. Antonangeli, J. Siebert, C. M. Aracne, D. L. Farber, A. Bosak, M. Hoesch, M. Krisch, F. J. Ryerson, G. Fiquet, and J. Badro, *Science* **331**, 64 (2011).
- [26] G. M. Manthilake, N. De Koker, D. J. Frost, and C. A. McCammon, *Proc. Natl. Acad. Sci. USA* **108**, 17901 (2011).
- [27] X. Tang and J. Dong, *Phys. Earth Planet. Inter.* **174**, 33 (2009).
- [28] H. Dekura and T. Tsuchiya, *Phys. Rev. B* **95**, 184303 (2017).
- [29] H. C. Ryu, M. H. Kwak, S. B. Kang, S. Y. Jeong, M. C. Park, K. Y. Kang, S. J. Lee, S. E. Moon, and S. O. Park, *Integr. Ferroelectr.* **95**, 83 (2007).
- [30] See Supplemental Material at <http://link.aps.org/supplemental/10.1103/PhysRevB.103.054302> for detailed methods and analysis [40–51].
- [31] P. Giura, L. Paulatto, F. He, R. P. S. M. Lobo, A. Bosak, E. Calandrini, L. Paolasini, and D. Antonangeli, *Phys. Rev. B* **99**, 220304(R) (2019).
- [32] H. A. Kramers, *Atti Cong. Intern. Fis. (Trans. Volta Centen. Congr.* **2**, 545 (1927).
- [33] R. de L. Kronig, *J. Opt. Soc. Am.* **12**, 547 (1926).
- [34] A. R. Oganov, M. J. Gillan, and G. D. Price, *J. Chem. Phys.* **118**, 10174 (2003).
- [35] D. Antonangeli, M. Krisch, D. L. Farber, D. G. Ruddle, and G. Fiquet, *Phys. Rev. Lett.* **100**, 085501 (2008).
- [36] E. Grüneisen, *Ann. Phys.* **344**, 257 (1912).
- [37] O. L. Anderson, *Geophys. J. Int.* **143**, 279 (2000).
- [38] J. Pellicer-Porres, A. Segura, C. Ferrer-Roca, J. A. Sans, and P. Dumas, *J. Phys.: Condens. Matter* **25**, 505902 (2013).
- [39] X. Yang, T. Feng, J. S. Kang, Y. Hu, J. Li, and X. Ruan, *Phys. Rev. B* **101**, 161202(R) (2020).
- [40] D. L. Farber, D. Antonangeli, C. M. Aracne, J. Benterou, *High Press. Res.* **26**, 1 (2006).
- [41] A. Celeste, F. Borondics, and F. Capitani, *High Press. Res.* **39**, 608 (2019).
- [42] P. Roy, M. Rouzières, Z. Qi, and O. Chubar, *Infrared Phys. Technol.* **49**, 139 (2006).

- [43] A. Voute, M. Deutsch, A. Kalinko, F. Alabarse, J.-B. Brubach, F. Capitani, M. Chapuis, V. Ta Phuoc, R. Sopracase, and P. Roy, *Vib. Spectrosc.* **86**, 17 (2016).
- [44] J. P. Perdew, K. Burke, and M. Ernzerhof, *Phys. Rev. Lett.* **77**, 3865 (1996).
- [45] M. Schlipf and F. Gygi, *Comput. Phys. Commun.* **196**, 36 (2015).
- [46] T. J. B. Holland and R. Powell, *J. Metamorph. Geol.* **29**, 333 (2011).
- [47] Y. Fei and Y. I. F. Ei, *Am. Mineral.* **84**, 272 (1999).
- [48] S. Speziale, C.-S. Zha, T. S. Duffy, R. J. Hemley, and H. Mao, *J. Geophys. Res. Solid Earth* **106**, 515 (2001).
- [49] M. Calandra, M. Lazzeri, and F. Mauri, *Physica C* **456**, 38 (2007).
- [50] L. Paulatto, F. Mauri, and M. Lazzeri, *Phys. Rev. B* **87**, 214303 (2013).
- [51] L. Paulatto, I. Errea, M. Calandra, and F. Mauri, *Phys. Rev. B - Condens. Matter Mater. Phys.* **91**, 054304 (2015).